Synthesis and characterization of spherical calcia stabilized zirconia nano-powders obtained by spray pyrolysis

H.E. Esparza-Ponce, A. Reyes-Rojas, W. Antúnez-Flores, M. Miki-Yoshida

Abstract

Fine, spherical $Ca_{0.15}Zr_{0.85}O_{1.85}$ nano-powders were prepared by spray pyrolysis, starting from a mixed aqueous and ethylic solution of zirconium acetylacetonate and calcium acetate. The influence of solution concentration, furnace temperature, mass flow of carrier gas and voltage of precipitator on microstructure, average particles size and recovery percentage were evaluated. The powders were synthesized without sintering, and for adequate preparation conditions, were mostly spherical, solid and narrowly size distributed. Average particle size ranges between 40 and 350 nm. Transmission electron micrographs showed that crystalline calcia stabilized zirconia particles were constituted by small crystallites, their size varying between 2 and 40 nm. X-ray diffraction analysis shows that powders obtained at low temperature were amorphous; for higher temperatures (~800 °C), it is found the presence of the tetragonal and cubic phases.

Introduction

Zirconia is one of the most promising ceramics for both structural and functional materials [1]. The stabilized zirconium oxide has many applications as a refractory ceramic at high temperature.

Spray pyrolysis [2] is a relatively low cost, simple to manipulate, applicable to large-scale production; which enables one to prepare homogeneous, spherical and narrowly size distributed ceramic powders. In the spray pyrolysis process, a starting

solution is pulverized by means of a carrier gas (e.g. compressed air) so that it arrives at the reactor in the form of very fine droplets. With adequate conditions, the precursor salts react to form the desired compound into the furnace. The chemical reactants are selected such that the undesirable products are volatile at the temperature of salt decomposition. The properties of the powders depend greatly on the preparation conditions, and can be easily tailored by adjusting or optimising the conditions that are suitable for a particular application. Particle size control can be easily achieved by varying the concentrations of the initial solution or the atomisation parameters. Different materials can be obtained by the spray pyrolysis method [3-6].

In this work, the preparation and structural characterization of calcia stabilized zirconia (CaSZ) powders by the spray pyrolysis technique are reported. The powders were recollected using an electrostatic precipitator. In particular, the influence of starting solution concentration, airflow, furnace temperature and high voltage of recollection on the microstructural characteristics and recollection efficiencies were analysed.

Experimental procedure

Zirconia based powder preparation: The spray pyrolysis system used in this work is shown in Fig. 1. It mainly consists of a pneumatic atomizer (a), in which the precursor solution is converted into a fine mist, and then it was carried out by the airflow and injected by a nozzle (b) into the quartz tube (c), which takes the place of a reaction chamber. The airflow was regulated with a mass flow controller (d). The solution temperature was controlled precisely (±1 °C) by partially immersing the solution container in a deionized water bath (e). The quartz tube was located inside a cylindrical furnace (f), which has a very precise temperature control (±1 °C). At this stage, with

optimal conditions (furnace temperature, chemical parameters, carrier gas nature and velocity), the particle growth mechanism develops: droplet evaporation and transport of reactants, gas phase diffusion of the reactants, chemical reaction, particle growth, structural arrangement, desorption of product gases, and evacuation of product gases. Finally, at the outermost side of the quartz tube, the electrostatic precipitator (g) is placed. This is composed of a recollection tube (h) and anode wire (i) connected to a high voltage source (j).

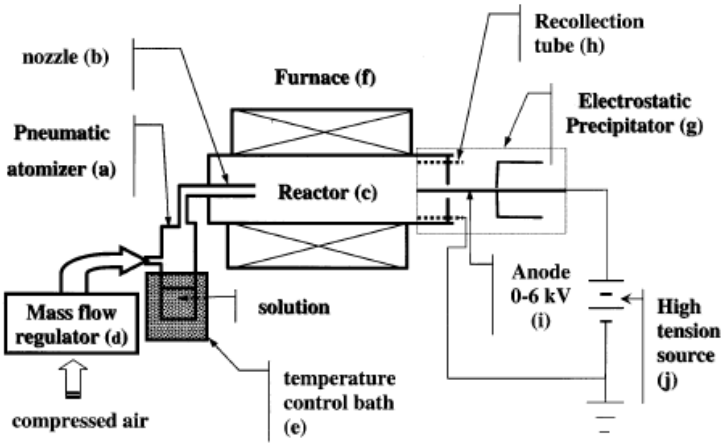

Fig. 1. Schematic diagram of the spray pyrolysis system utilized to prepare zirconia based nano-powders.

CaSZ $Zr_{0.85}Ca_{0.15}O_{1.85}$ powders were also prepared from a solution of $Zr[CH_3COCH=C\text{-}O\text{-}CH_3]_4$ and $Ca(CH_3COO)_2{\cdot}H_2O$ in a mixture of 60% deionized water and 40% absolute ethanol. A Zr-Ca molar proportion of 0.86:0.14 was chosen and total precursor concentrations of 0.01, 0.05 and 0.1 mol dm^{-3} were tested. The furnace temperature tried was 800, 900 and 1000 °C; different carrier gas flows were tested from 33 to 167 $cm^3\ s^{-1}$ (2, 4, 5, 6, 8 and 10 $dm^3\ min^{-1}$); precipitator high voltage was

varied between 0 and 6 kV (0, 2, 4.6 and 6 kV). Some samples were obtained controlling the solution bath temperature at 50 °C.

Powder characterization: The crystal structure of the powders was analysed by X-ray diffraction (XRD) collected in an automatic D5000 diffractometer, using a Cu Kα (λ=1.54056 Å) source operating at 40 kV and 30 mA, with a graphite monochromator. Data were collected in the 2θ ranges from 5 to 100°, in step-scanning mode, with a step of 0.05° and a counting time of 5 s per step. The crystallite size of powders obtained at 900 8C, solution concentration of 0.05 mol dm^{-3} and airflow of 4, 6, 8 and 10 dm^3 min^{-1} were calculated with the (111)c diffraction peak, using the Scherrer's relation [7] $D=0.9\lambda(\beta \cos \theta)^{-1}$, the line broadening β was calculated as the difference between the observed β_{obs} broadening and the instrumental broadening β_{inst}. The instrumental broadening was predetermined from the XRD spectrum of Al_2O_3, a well-known standard.

The particle microstructure was analysed by electron microscopy, using a JSM 5800LV scanning and a CM200 transmission electron microscopes, both equipped with a DX prime energy dispersive X-ray spectrometer (EDS). From these analyses, particle composition, morphology, and crystalline structure were obtained as a function of the preparation conditions.

In addition, the average particle size (APS) was evaluated as function of the airflow, solution concentration and furnace temperature. For the determination of the APS of each sample, around 200 particles were measured directly from several bright field transmission electron micrographs, using digital imaging analyser IMAGE-PRO PLUS 4.1. Finally, the partial recovery percentage (PRP) was measured taking the ratio

of powder mass actually recollected in the precipitator to that contained in the total consumed solution if all the precursor salt was transformed to zirconium oxide. The PRP was also evaluated as a function of the experimental conditions.

Results

Microstructure of ZrO_2-CaO fine powders: Fig. 2 shows typical XRD spectrum of the CaSZ powders. Only, diffraction peaks corresponding to the cubic [8] and tetragonal [9] phases were detected indicating that a partially stabilized structure has been formed, as suggested also by selected area electron diffraction (SAED) results. Table 1 shows interplanar distance calculated from SAED patterns of CaSZ powders, obtained at 900 °C; 0.05 mol dm^{-3}; 4.6 kV; and different airflow (A 4; B 6; C 8; and D 10 dm^3 min^{-1}).

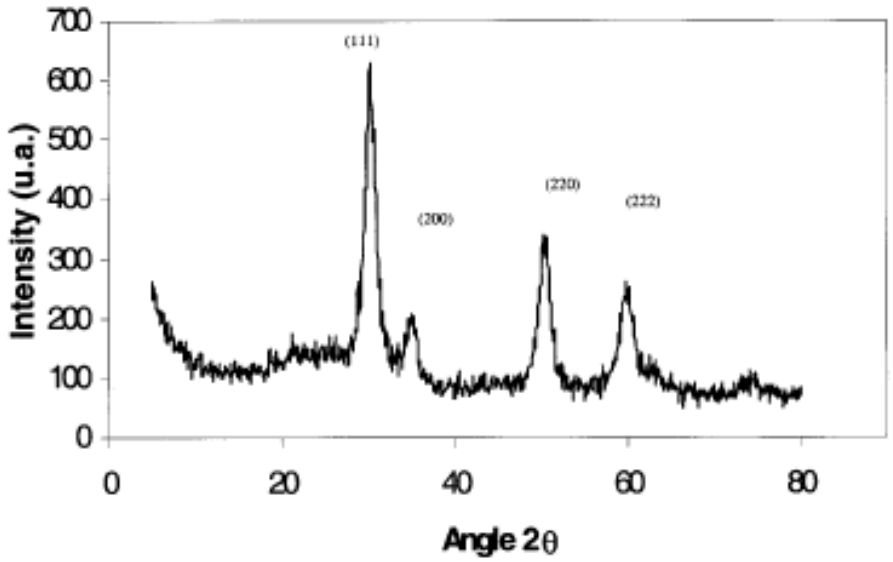

Fig. 2. Typical XRD spectra of CaSZ.

Table 1
Interplanar distance obtained from SAED patterns of several CaSZ powders analysed in this work

Phase	*h*	*k*	*l*	*d* (nm) ICDD	*d* (nm) experimental A	*d* (nm) experimental B	*d* (nm) experimental C	*d* (nm) experimental D
Cubic	1	1	1	0.2961	0.2968	0.2968	0.2986	0.2986
Tetragonal	1	1	0	0.2574	0.2626	0.2586	0.2572	0.2586
Tetragonal	1	1	2	0.1841	0.1844	0.1824	0.1851	0.1831
Cubic	3	1	1	0.1548	0.1553	0.1548	0.1558	0.1553
Cubic	4	0	0	0.1284	–	–	–	0.1239

It can be concluded, the presence of cubic and tetragonal phases. The estimation, by the Rietveld method, of the proportion of these phases indicated that up to 5 wt.% of tetragonal phase was present.

SEM micrograph representative of CaSZ powder is shown in Fig. 3. It can be observed that spherical particles were the predominant morphology; only a small number of them show a hollow or irregular shape. Other important characteristics of the powders obtained by this method were that the aggregation-free particles had a narrowly size distribution around 57 nm.

Fig. 4 shows transmission electron microscopy (TEM) micrographs of the powders prepared at 900 °C, solution concentration of 0.05 mol dm^{-3} and different air flow (4, 6, 8 and 10 dm^3 min^{-1}). It can be seen that most of the particles are spherical, with their size decreasing as the airflow increases; in addition, certain morphology change was observed for high airflow samples (8 and 10 dm^3 min^{-1}), they show irregular shaped particles. Furthermore, each particle consists of many small crystallites (<10 nm), which could be outlined by their lattice fringes, as it is shown in Fig. 5. The observed lines correspond to (200) planes of cubic phase.

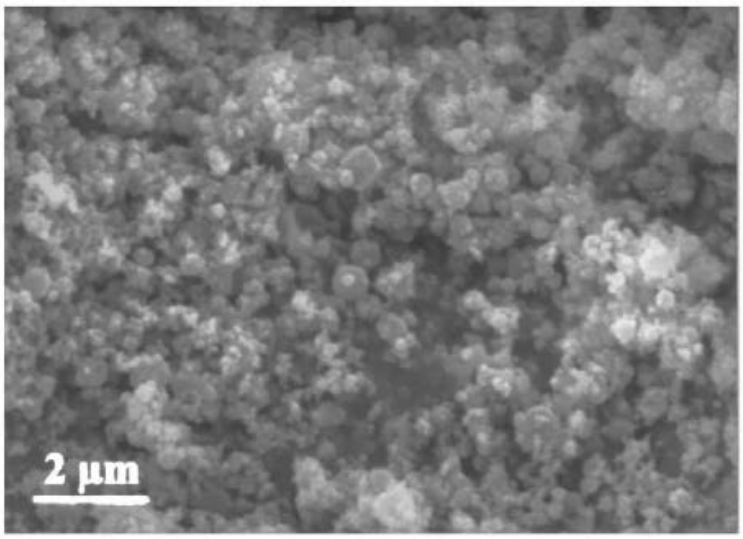

Fig. 3. Secondary electron SEM micrograph of CaSZ powder obtained from a 0.05 mol dm^{-3} solution, at 900 °C, with an airflow of 5 dm^3 min^{-1} and deposition time of 30 min.

The crystallite size size estimated from XRD analysis was almost constant for these samples, in the range between 4 and 6 nm.

Effect of airflow on the APS of CaSZ powders: It is worthwhile to consider that the APS measured in all the samples of CaSZ prepared in this work was nanometric, in the range from 40 to 350 nm. The APS was also considerably smaller than those calculated from the average droplet size using a known approach [2] (see Table 2). The occurrence of this small APS can be probably attributed to both the break down of the droplet and/or precursor salt evaporation, as will be discussed later.

Fig. 6 shows the dependence of the APS as a function of: (a) airflow; and (b) furnace temperature. The conditions tried were solution concentration of 0.05 and 0.1 mol dm^{-3}, without solution bath temperature control. The other fixed conditions, for airflow dependence, were furnace temperature of 900 °C and precipitator voltage of 4.6 kV. It can be concluded that the APS initially increases with the growth of airflow from 2

to 8 dm3 min^{-1}, then for a further increase of the airflow, there is stagnation or a decrease of the APS. The overall tendency of the APS is to decrease when the temperature increases from 800 to 900 °C; then, for a further increase of the temperature, the APS is almost constant or shows a slight increase.

Fig. 7 shows that inner crystallite size grows as furnace temperature increases and airflow decreases. Fig. 7a and b show bright field TEM micrographs of powders obtained at 900 and 1000 °C, respectively (6 dm^3 min^{-1}, 4.6 kV, 0.1 mol dm^{-3}). In this case, it can be noted a slight increment of crystallite size, from 2-6 to 3-8 nm approximately. In contrast, for samples obtained at 900 °C and airflow of 2 dm^3 min^{-1}, the crystallite size increases to 24-41 nm (see Fig. 7c).

Effect of preparation conditions on the PRP of CaSZ powders: Fig. 8a shows the PRP as a function of the airflow; from solutions of 0.05 and 0.1 mol dm^{-3}, it is observed an increase of the PRP as the airflow increases, ranging between 3 and 10 wt.%. This trend can be related to the fact that high airflow can drag bigger particles with more weight; which is consistent with the experimental variation of APS through the airflow.

As expected, the PRP increases when the voltage of precipitator increases. The sampling efficiency of the electrostatic precipitator is mainly governed by the particle transport due to the flow and the electrostatic field; therefore, high electrostatic field increases the recovery (Fig. 8b). It is worthwhile to mention that the voltage of precipitator limits the values of PRP, since no more high voltage can be applied due to electrical discharges in the precipitator. It is also observed that the electrostatic precipitator collects more small particles with the increment of the voltage.

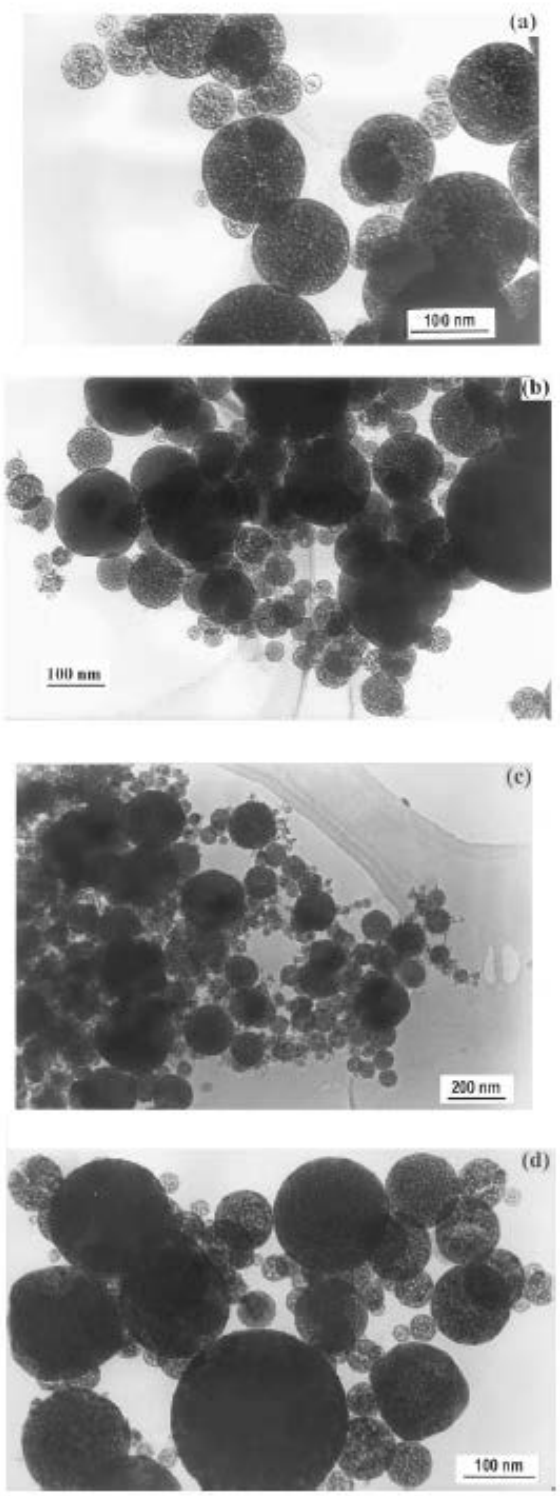

Fig. 4. Bright field TEM micrographs of CaSZ obtained at 900 °C, solution concentration of 0.05 mol dm^{-3} and airflow of: (a) 4; (b) 6; (c) 8; and (d) 10 dm^3 min^{-1}.

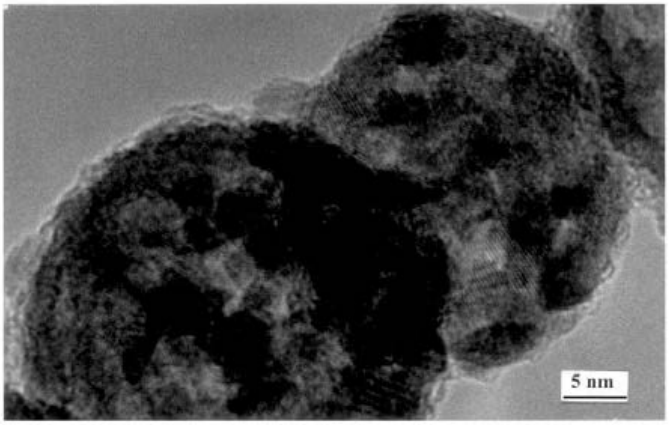

Fig. 5. High resolution TEM micrograph showing a lattice fringe image of CaSZ particles obtained at 900 °C.

Table 2
Mean droplet diameter (d), critical diameter (d_c), expected maximum particle diameter (D), and estimated residence time (τ) of sprayed droplets as a function of airflow (ϕ_A)

ϕ_A (dm^3 min^{-1})	d (μm)	d_c (μm)	D (μm)	τ (s)
2	119	16	2.1	16.3
4	60	24	3.1	8.1
5	47	27	3.5	6.5
6	40	30	3.9	5.4
8[a]	30	36	3.9	4.1
10[a]	24	42	3.1	3.3

Discussion

In the next paragraphs, the influence of experimental conditions, such as: airflow, solution concentration, furnace temperature and voltage of precipitator, on relevant characteristics of the obtained powders as morphology, APS, crystalline structure and PRP are considered. This influence will be discussed considering that, in general, the growth and micro-structural characteristics of the powders prepared by spray pyrolysis are determined by the combined effect of the droplet size effectively transported (d_e) to the reaction chamber, the residence time (T) and the rate of droplet heating (R_H) in the chamber.

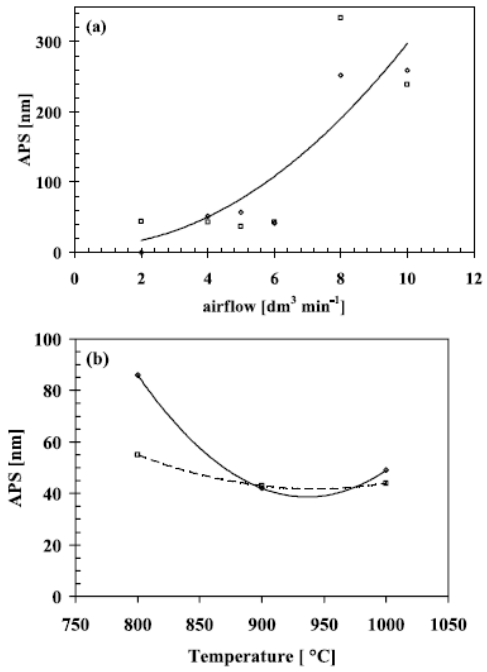

Fig. 6. APS as function of: (a) airflow; and (b) furnace temperature. For 0.05 (◆) and 0.1 (■) mol dm^{-3} solutions without heating.

It is well established, for conventional pneumatic spraying, i.e. if the sprayed droplets are focussed directly towards the reaction chamber, the droplets size decreases when the airflow increases [2]. However, in our system, the atomizer sprays down to the solution container and the mist of solution is carried out in the upward direction by the airflow. In this configuration occurs a droplet size selection due to the combined effect of gravitational and Stokes' forces [10]. When these forces reach equilibrium, the droplet travel with a constant terminal velocity, which is a function of the particle size. Therefore, only the droplets smaller than certain critical size can be carried out to the reaction chamber. This critical size (d_e) is airflow dependent. For our particular system, at low and medium airflow ($0<\Phi_A<8$ dm^3 min^{-1}) in fact the reliance between droplet size and airflow was reversed, i.e. average droplet size increases with the increase of airflow. Only, if the carrier gas flow increases further ($\Phi_A \geq 8$ dm^3 min^{-1}) any

selection happens; and the average droplet size decreases with the increase of airflow. Table 2 shows the values of de calculated as a function of airflow, for a 0.1 mol dm^{-3} solution.

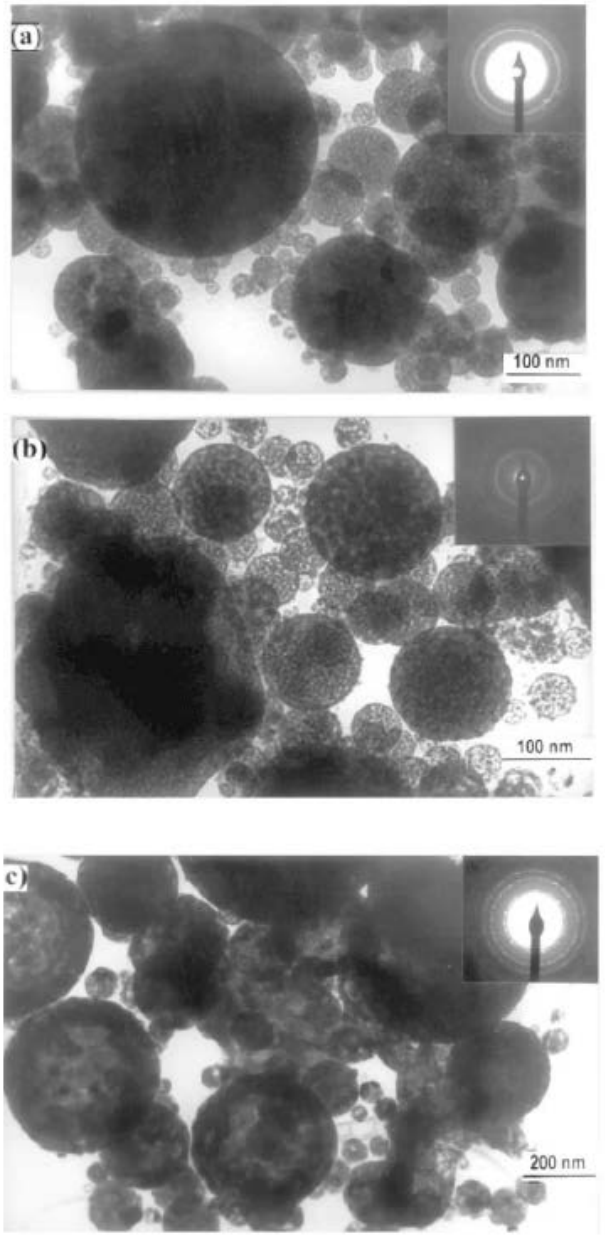

Fig. 7. Bright field TEM micrographs of CaSZ obtained at: (a) 900 °C, airflow 6 dm^3 min^{-1}; (b) 1000 °C, airflow 6 dm^3 min^{-1}; and (c) 900 °C and airflow 2 dm^3 min^{-1}. The solution concentration was 0.1 mol dm^{-3}, and precipitator voltage 4.6 kV.

The residence time (T) of the droplets, in the region of high temperature of the cylindrical furnace, was also estimated as a function of the carrier gas flow rate (ΦA), taking into account the geometry of the reactor. No gas expansion correction was considered in this assessment; then the real residence time may be 25 times smaller, as estimated since the work of Milosevic et al. [11]. These results are also tabulated in Table 2. Subsequently, at a fixed furnace temperature the residence time decreased when airflow increased. In addition, the rate of droplet heating (R_H) has been estimated considering the furnace temperature distribution, airflow rate and geometry of the reaction chamber. It can be concluded that, under the experimental conditions utilized in this work, a very high increase of the heating rate (thousands of °C s^{-1}) happens when the airflow increases.

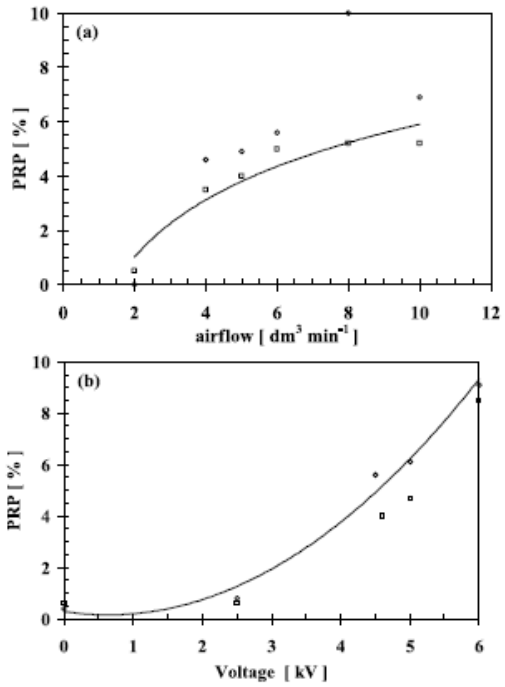

Fig. 8. PRP as a function of: (a) airflow (900 °C, 4.6 kV); and (b) voltage of precipitator (900 °C, 6 dm^3 min^{-1}). For 0.05 (◆) and 0.1 (■) mol dm^{-3} solutions without heating.

The APS measured in the samples prepared in this work was considerably smaller than those calculated from the critical or average droplet size (see Table 2). This result can be explained by two possible mechanisms. The first, considering that each droplet did not convert to a unique particle, due to the occurrence of an important droplet break down [2] and/or an explosive boiling [12]. These events presumably were produced when the droplets travel into the nozzle before they have been injected to the reaction chamber. At this stage, the residence time (~10^{-3} s) is shorter than the drying time (~0.1 s [11]) and the heating rate is very high (> 10^5 °C s^{-1}), in these conditions a vigorous boiling of the droplets can happen, given as a consequence the break down of the droplets. The second additional mechanism can occur after dehydration of the droplet/particle, at the beginning of their travel in the quartz tube. Due to the high temperature and very large surface area of the precursor salt particles, the total evaporation rate can be extremely high, given as a consequence the loose of the precursor material or the formation of many ultra fine particles. This mechanism was also suggested for ZnO powders by Liu et al. [4]. It is expected that precursor evaporation was more intense at low airflow, i.e. when the residence time in the reaction chamber was high. Moreover, at high solution concentration the droplets tend to evaporate the solvent more quickly, thus, they formed precursor salt particles more easily and consequently the precursor evaporation rate increased. The experimental results are consistent with these two considerations. First, the APS was low for airflow smaller than 6 dm^3 min^{-1} (see Fig. 6a); additionally, the APS decreased with the increase o solution concentration (see Fig. 6b). The fact that the

PRP was low also suggests that a high proportion of precursor material is lost by the evaporation of it. Furthermore, the variation of PRP with the airflow and, solution concentration is consistent with these arguments. It observed a decrease of the PRP for low airflows (see Fig. 7a), i.e. when the residence time increases and consequently, the evaporation rate of precursor salt increases. On the other hand, the decrease of the PRP is congruent with the increase of the evaporation rate as the solution concentration increases.

The formation of hollow particles can be related to the localized super-saturation of the solute with the consequent formation of a crust on the droplets surface [13]; which depends on the evaporation rate of the solvent, and on the strength and permeability of the crust. When the concentration of precursor solution is high enough, the crust is formed earlier on the droplet surface. The internal solvent, encapsulated by the forming crust, expands when heated and increases the particle size of the powder; given rise after the complete evaporation of solvent to hollow particles that can break into irregular particles. It is believed that the influence of the residence time is higher when it is shorter than the time needed for complete evaporation of the solvent. In that case, for high enough airflow, the particle size tends to grow, because the formation of crust occurs earlier by the cooperative effect of low T and high R_H.

Conclusions

It has been demonstrated the feasibility to produce CaSZ nano-powders without post-heat treatment with the spray pyrolysis technique. Compared with the traditional method, the powders are obtained in one step, saving time and energy. The powders were synthesized without sintering, and for adequate preparation conditions, were

mostly spherical, solid and narrowly size distributed. The composition of CaSZ powders obtained without heating the precursor solution corresponds to the molar proportion of precursor salts in solution. Below 650 °C, the powders were amorphous; for higher temperatures it is found that the tetragonal and cubic phases were present. The size, morphology, and structural characteristics of zirconia and CaSZ powders depend principally on the source solution concentration, reaction chamber temperature, and airflow.

Acknowledgements

We are very grateful to D. Lardizabal, F. Paraguay D., and K. Go´mez F. for experimental assistance.

References

[1] T. Uchikoshi, Y. Sakka, K. Ozawa, K. Hiraga, Mat. Res. Soc. Symp. Proc. Vol. 520, Materials Research Society, 1998.

[2] K. Okada, A. Tanaka, S. Hayashi, N. Otsuka, J. Mater. Sci. Lett. 12 (1993) 854.

[3] M. Vallet-Regí, L.M. Rodríguez-Lorenzo, C.V. Ragel, A.J. Salinas, J.M. Gonza´lez-Calbet, Solid State Ionics 101-103 (1997) 197.

[4] Tian-Quan Liu, Osamu Sakurai, Nobuyasu Mizutani, Masanori Kato, J. Mater. Sci. 21 (1986) 3698.

[5] Jong-Heun Lee, Soon-Ja Park, J. Am. Ceram. Soc. 76 (3) (1993) 777.

[6] O. Milosevic, B. Jordovic, D. Uskokovic, Mater. Lett. 19 (1994) 165.

[7] E.F. Kaelble (Ed.), Handbook of X-rays, Part 2 (Chapter 17), McGraw-Hill, New York, 1967.

[8] Powder Diffraction File, Joint Committee on Powder Diffraction Standards, International Center for Diffraction Data, Swarthmore, PA, 1996, card 26-0341.

[9] Powder Diffraction File, Joint Committee on Powder Diffraction Standards, International Center for Diffraction Data, Swarthmore, PA, 1996, card 42-1164.

[10] M. Miki-Yoshida, E. Andrade, Thin Solid Films 224 (1993) 87.

[11] O. Milosevic, et al., Thin Solid Films 296 (1997) 44.

[12] M. Shusser, T. Ytrehus, D. Weihs, Fluid Dyn. Res. 27 (2000) 353.

[13] S.Y. Cho, J.H. Lee, S.J. Park, J. Mater. Sci. 30 (1995) 3274-3278.